Infrared cutoff for dipolar droplets

He, Liang Jun; Maucher, Fabian; Zhang, Yong Chang

DOI
10.1103/PhysRevA.110.053316

Publication date
2024

Document Version
Final published version

Published in
Physical Review A

Infrared cutoff for dipolar droplets

Liang-Jun He,[1] Fabian Maucher,[2] and Yong-Chang Zhang[1,*]

[1]*MOE Key Laboratory for Nonequilibrium Synthesis and Modulation of Condensed Matter, Shaanxi Key Laboratory of Quantum Information and Quantum Optoelectronic Devices, School of Physics, Xi'an Jiaotong University, Xi'an 710049, People's Republic of China*

[2]*Faculty of Mechanical, Maritime and Materials Engineering; Department of Precision and Microsystems Engineering, Delft University of Technology, 2628 CD, Delft, The Netherlands*

(Received 3 July 2024; revised 9 October 2024; accepted 29 October 2024; published 18 November 2024)

The beyond mean-field physics due to quantum fluctuations is often described with the Lee-Huang-Yang correction, which can be approximately written as a simple analytical expression in terms of the mean-field wave function employing local density approximation. This model has proven to be very successful in predicting the dynamics in dipolar Bose-Einstein condensates both qualitatively and quantitatively. Yet a small deviation between experimental results and the theoretical prediction has been observed when comparing experiment and theory of the phase boundary of a free-space quantum droplet. For this reason we revisit the theoretical description of quantum fluctuations in dipolar quantum gases. We study alternative cutoffs, compare them to experimental results, and discuss limitations.

DOI: 10.1103/PhysRevA.110.053316

I. INTRODUCTION

Particles in dilute dipolar Bose-Einstein condensates (BECs) interact with contact interaction via *s*-wave scattering as well as long-range dipole-dipole interaction (DDI). Because of the anisotropic nature of the DDI, the mean-field effect becomes comparable to beyond mean-field contributions related to quantum fluctuations. This leads to a range of interesting and unexpected phenomena, such as self-bound quantum droplets [1–13], supersolidity and superfluidity [14–38], excitations [39,40], and quench dynamics [19,25–30,41,42]. Similarly, beyond mean-field behavior has also been discussed and observed in binary BECs [43–52].

The beyond mean-field corrections caused by quantum fluctuations to the mean field were first theoretically introduced by Lee, Huang, and Yang [53,54]; therefore, they are referred to as the Lee-Huang-Yang (LHY) correction. The LHY correction can take different forms depending on the characteristics of the underlying physics, such as the range of interactions [43,44,55–57], the dimensionality [43,44,56–58], multicomponents [8,9], and gauge fields [59–62]. By incorporating the LHY correction into the usual Gross-Pitaevskii equation (GPE), one can obtain an extended Gross-Pitaevikii equation (eGPE) [43,44,56,57,63–65]. The eGPE successfully predicted the emergence of quantum droplets in binary and dipolar BECs [2–10,43–45]. Moreover, the eGPE also provided a deeper understanding of the excitation spectrum [39,40,66–75] and supersolid states [10–41,76,77] as well as other remarkable phenomena arising in quantum gases that cannot be understood on the mean-field level.

These experimental observations are in good agreement with the theoretical description in both binary and dipolar BECs, which demonstrates that the eGPE description is a powerful tool to describe a range of phenomena quite accurately. Yet, there remains a quantitative deviation between the theoretical prediction and experimental results [6,45,78].

With respect to quantum droplets, we can distinguish two situations: either the BECs can form a self-bound droplet state in free space or the BECs delocalize towards ultimately forming a plane wave, depending on the interaction strength and particle number. The critical line between these two phases predicted by the eGPE exhibits an evident shift towards either weaker repulsive short-ranged interaction or larger particle number as compared to the experimental results for dipolar BECs [6]. This mismatch between theory and experiment might be caused by the approximations used for the derivation of the LHY correction, which are most importantly the local density approximation and the infrared cutoff in momentum space.

A way to avoid having to make a cutoff is resorting to the time-dependent Hartree-Fock-Bogoliubov (TDHFB) equations rather than the eGPE. The results obtained numerically by solving the TDHFB equations feature a good agreement with experimental results at relatively small particle numbers in dipolar BECs [79]. However, whereas the TDHFB equations represent a quite accurate tool to investigate the beyond mean-field physics, they are numerically expensive to solve, particularly when considering systems with more than one spatial dimension. Therefore, it remains desirable to explore simple and nearly analytical approaches to describe the effect of quantum fluctuations as well as possible.

A numerically cheaper avenue is to reformulate the LHY correction slightly, at the cost that the cutoff becomes spatially dependent. To derive the LHY correction, usually one calculates the Bogoliubov excitation spectrum assuming that variations in the wave function itself are slow compared to

*Contact author: zhangyc@xjtu.edu.cn

excitations. Therefore, one can calculate the spectrum for an unmodulated state without explicit dependence on spatial dimensions and later add the spatial dependence of the wave function. This method is commonly referred to as local density approximation [56,57,63–65]. It becomes less applicable once the two scales become comparable.

Due to the attractive part of the DDI, the excitation spectrum of dipolar BECs is complex in the low-momentum regime and, thus, leads to a finite imaginary part of the LHY correction. This can be neglected to a certain extent [80]. Considering that a finite size of BECs inherently imposes a threshold on the low momenta of allowed excitations, it was suggested to reformulate the LHY correction by taking a cutoff in momentum space [4,77,80].

In this paper we will compare different cutoffs, their impact on the LHY correction and the subsequent shift of the droplet phase boundary, and their comparison to the experimental data. Among the cutoffs we discuss, we choose the healing length as a natural length scale to the momentum cutoff and show that it leads to an improved agreement to the experimental data.

The paper is organized as follows. In Sec. II A we present the derivation of the LHY correction via Hartree-Fock-Bogoliubov (HFB) theory to provide context [56,57,63–65,81,82]. In Sec. II B we propose a cutoff associated with the healing length to reformulate the LHY correction and compare it with other possible types of cutoffs. In Sec. III we compare the theoretical result obtained by employing different cutoffs for the LHY correction to the experimental observations and furthermore discuss the contributions of low-energy discrete excitations of a self-bound droplet [66]. Section IV provides a conclusion.

II. FORMULATION OF LHY CORRECTION

A. LHY correction

We consider a three-dimensional ultracold quantum gas in free space, where the particles interact via short-range repulsion as well as long-range DDI as

$$V(\mathbf{x}) = g\left[\delta(\mathbf{x}) + \frac{3\epsilon_{\rm dd}}{4\pi|\mathbf{x}|^3}\left(1 - 3\frac{z^2}{|\mathbf{x}|^2}\right)\right]. \tag{1}$$

Here $g = \frac{4\pi\hbar^2 a_s}{M}$ with M being the atomic mass, and $\epsilon_{\rm dd} = \frac{a_{\rm dd}}{a_s}$. a_s is the s-wave scattering length and can be tuned via Feshbach resonances [6,83–85], while $a_{\rm dd} = \frac{\mu_0 d^2 M}{12\pi\hbar^2}$ represents the dipolar length [2,6,57] with μ_0 and d being the vacuum permeability and the magnetic dipole moment, respectively. The dynamics of such a system is governed by the following Hamiltonian:

$$\hat{H} = \int \mathrm{d}^3\mathbf{x}\hat{\psi}^\dagger(\mathbf{x})h_0(\mathbf{x})\hat{\psi}(\mathbf{x}) + \frac{1}{2}\iint \mathrm{d}^3\mathbf{x}\mathrm{d}^3\mathbf{x}'\hat{\psi}^\dagger(\mathbf{x})\hat{\psi}^\dagger(\mathbf{x}')V(\mathbf{x}-\mathbf{x}')\hat{\psi}(\mathbf{x}')\hat{\psi}(\mathbf{x}), \tag{2}$$

where $h_0(\mathbf{x}) = -\frac{\hbar^2\nabla^2}{2M} - \mu$ is the single-particle Hamiltonian containing the kinetic energy and the chemical potential μ, and $\hat{\psi}(\mathbf{x})$ denotes the field operator of particles. According to the HFB theory, the field operator can be approximately expanded as

$$\hat{\psi}(\mathbf{x}) = \Psi(\mathbf{x}) + \hat{\phi}(\mathbf{x}) \tag{3}$$

with $\Psi(\mathbf{x}) = \langle\hat{\psi}(\mathbf{x})\rangle$ being the mean-field value and $\hat{\phi}(\mathbf{x})$ representing the operator of fluctuations with $\langle\hat{\phi}\rangle = 0$.

By substituting this expansion into the above Hamiltonian, keeping up to the third order with respect to the fluctuation operator and combining the third-order terms into the first-order term via Hartree-Fock factorization (see Appendix A for details), eventually one can obtain the following equation by setting the corresponding coefficient be equal to zero since the first-order term must vanish for the ground state [64,65,86]:

$$\left[h_0(\mathbf{x}) + \int \mathrm{d}^3\mathbf{x}'V(\mathbf{x}-\mathbf{x}')|\Psi(\mathbf{x}')|^2\right]\Psi(\mathbf{x}) + \int \mathrm{d}^3\mathbf{x}'V(\mathbf{x}-\mathbf{x}')\tilde{n}(\mathbf{x}',\mathbf{x}')\Psi(\mathbf{x}) + \int \mathrm{d}^3\mathbf{x}'V(\mathbf{x}-\mathbf{x}')\tilde{n}(\mathbf{x}',\mathbf{x})\Psi(\mathbf{x}') + \int \mathrm{d}^3\mathbf{x}'V(\mathbf{x}-\mathbf{x}')\tilde{m}(\mathbf{x}',\mathbf{x})\Psi^*(\mathbf{x}') = 0, \tag{4}$$

i.e., a stationary eGPE. The first line corresponds to the usual mean-field GPE, while the additional terms describe the contributions of quantum fluctuations and can be reformulated into the LHY correction as will be discussed later. To obtain this eGPE, we have assumed that the dipolar gas is in the ground state with the corresponding wave function $\Psi(\mathbf{x})$, and we have defined the noncondensate density $\tilde{n}(\mathbf{x}',\mathbf{x}) = \langle\hat{\phi}^\dagger(\mathbf{x}')\hat{\phi}(\mathbf{x})\rangle$ and anomalous noncondensate density $\tilde{m}(\mathbf{x}',\mathbf{x}) = \langle\hat{\phi}(\mathbf{x}')\hat{\phi}(\mathbf{x})\rangle$.

Due to the dependence on the noncondensate densities, it is not yet straightforward to deal with the ground-state dipolar BECs using Eq. (4). To further simplify the above eGPE, one needs to investigate the excitation spectrum as follows. By using the Bogoliubov transformation, the fluctuation operator can be written as $\hat{\phi}(\mathbf{x}) = \sum_j[u_j(\mathbf{x})\hat{\alpha}_j - v_j^*(\mathbf{x})\hat{\alpha}_j^\dagger]$, where $\hat{\alpha}_j$ ($\hat{\alpha}_j^\dagger$) is the annihilation (creation) operator of the quasiparticles and satisfy bosonic commutation relations. The Bogoliubov amplitudes are subject to the following constraint $\int \mathrm{d}^3\mathbf{x}[u_j^*(\mathbf{x})u_k(\mathbf{x}) - v_j^*(\mathbf{x})v_k(\mathbf{x})] = \delta_{jk}$ and can be determined by the Bogoliubov-de Gennes (BdG) equations as

$$\begin{aligned}
&\mathcal{L}_0 u_j(\mathbf{x}) + \int \mathrm{d}^3\mathbf{x}'V(\mathbf{x}-\mathbf{x}')\Psi^*(\mathbf{x}')\Psi(\mathbf{x})u_j(\mathbf{x}') - \int \mathrm{d}^3\mathbf{x}'V(\mathbf{x}-\mathbf{x}')\Psi(\mathbf{x}')\Psi(\mathbf{x})v_j(\mathbf{x}') = E_j u_j(\mathbf{x}) \\
&\mathcal{L}_0 v_j(\mathbf{x}) + \int \mathrm{d}^3\mathbf{x}'V(\mathbf{x}-\mathbf{x}')\Psi(\mathbf{x}')\Psi^*(\mathbf{x})v_j(\mathbf{x}') - \int \mathrm{d}^3\mathbf{x}'V(\mathbf{x}-\mathbf{x}')\Psi^*(\mathbf{x}')\Psi^*(\mathbf{x})u_j(\mathbf{x}') = -E_j v_j(\mathbf{x})
\end{aligned} \tag{5}$$

with $\mathcal{L}_0 = h_0(\mathbf{x}) + \int \mathrm{d}^3\mathbf{x}'V(\mathbf{x}-\mathbf{x}')|\Psi(\mathbf{x}')|^2$. By incorporating the Bogoliubov amplitudes obtained from the above BdG equations into the fluctuation operator, one can readily rewrite

the noncondensate densities as

$$\tilde{n}(\mathbf{x}',\mathbf{x}) = \sum_j \{v_j(\mathbf{x}')v_j^*(\mathbf{x}) + N_{\rm B}(E_j)[u_j^*(\mathbf{x}')u_j(\mathbf{x}) + v_j(\mathbf{x}')v_i^*(\mathbf{x})]\},$$
$$\tilde{m}(\mathbf{x}',\mathbf{x}) = -\sum_j \{u_j(\mathbf{x}')v_j^*(\mathbf{x}) + N_{\rm B}(E_j)[v_j^*(\mathbf{x}')u_j(\mathbf{x}) + u_j^*(\mathbf{x}')v_j(\mathbf{x})]\}, \quad (6)$$

where we have utilized the Bose statistics of the quasiparticles, i.e., $\langle\hat{\alpha}_j^\dagger\hat{\alpha}_k\rangle = \delta_{jk}N_{\rm B}(E_j)$ and $\langle\hat{\alpha}_j\hat{\alpha}_k\rangle = \langle\hat{\alpha}_j^\dagger\hat{\alpha}_k^\dagger\rangle = 0$ with $N_{\rm B}(E) = (e^{\beta E}-1)^{-1}$ and $\beta = k_{\rm B}T$. Now we arrive at the closed Eqs. (4)–(6), which are usually referred to as HFB theory. These equations can be solved self-consistently; however, the calculation is quite tough even for a homogeneous flat state and one usually has to resort to numerics [79].

To get around the complicated computation of the above HFB equations and reach a simple description of the effect of quantum fluctuations, one viable route is to employ the local-density approximation (LDA) [56,57,64,65,82] through the following substitutions:

$$u_j(\mathbf{x}) \to u(\mathbf{x},\mathbf{k})e^{i\mathbf{k}\cdot\mathbf{x}}, \quad v_j(\mathbf{x}) \to v(\mathbf{x},\mathbf{k})e^{i\mathbf{k}\cdot\mathbf{x}},$$
$$E_j \to E(\mathbf{x},\mathbf{k}), \quad \sum_j \to \int \frac{d^3\mathbf{k}}{(2\pi)^3}, \quad (7)$$

where $u(\mathbf{x},\mathbf{k})$ and $v(\mathbf{x},\mathbf{k})$ are slowly varying functions of $\mathbf{x}$ and are subject to the constraint $|u(\mathbf{x},\mathbf{k})|^2 - |v(\mathbf{x},\mathbf{k})|^2 = 1$. Under such an LDA, the BdG equation (5) can be solved analytically and results in the excitation spectrum and amplitudes as follows:

$$E(\mathbf{x},\mathbf{k}) = \sqrt{\varepsilon_{\mathbf{k}}[\varepsilon_{\mathbf{k}} + 2n_0(\mathbf{x})\tilde{V}(\mathbf{k})]},$$
$$|v(\mathbf{x},\mathbf{k})|^2 = \frac{\varepsilon_{\mathbf{k}} + n_0(\mathbf{x})\tilde{V}(\mathbf{k}) - E(\mathbf{x},\mathbf{k})}{2E(\mathbf{x},\mathbf{k})},$$
$$u(\mathbf{x},\mathbf{k})v^*(\mathbf{x},\mathbf{k}) = \frac{n_0(\mathbf{x})\tilde{V}(\mathbf{k})}{2E(\mathbf{x},\mathbf{k})} \quad (8)$$

with $\varepsilon_{\mathbf{k}} = \frac{\hbar^2\mathbf{k}^2}{2M}$, $n_0(\mathbf{x}) = |\Psi(\mathbf{x})|^2$, and $\tilde{V}(\mathbf{k}) = g[1 + \epsilon_{\rm dd}(3\cos^2\theta - 1)] = \tilde{V}(\theta)$ being the Fourier transformation of the interaction potential (1). Here we see that Fourier transform of the dipolar interaction depends only on the angle θ and not on all three components of $\mathbf{k}$ as can be expected from the azimuthal symmetry in direct space.

One can notice that the additional terms associated with fluctuations in Eq. (4) act like a shift of the chemical potential $\Delta\mu$ to the mean-field value μ:

$$\Delta\mu\Psi(\mathbf{x}) = \int d^3\mathbf{x}'V(\mathbf{x}-\mathbf{x}')\tilde{n}(\mathbf{x}',\mathbf{x})\Psi(\mathbf{x}') + \int d^3\mathbf{x}'V(\mathbf{x}-\mathbf{x}')\tilde{m}(\mathbf{x}',\mathbf{x})\Psi^*(\mathbf{x}'). \quad (9)$$

Employing LDA, this chemical potential shift can be expressed as

$$\Delta\mu(\mathbf{x}) = \int \frac{d^3\mathbf{k}}{(2\pi)^3}\tilde{V}(\mathbf{k})\{|v(\mathbf{x},\mathbf{k})|^2 - u(\mathbf{x},\mathbf{k})v^*(\mathbf{x},\mathbf{k}) + N_{\rm B}(E)[|u(\mathbf{x},\mathbf{k})|^2 + |v(\mathbf{x},\mathbf{k})|^2 - 2u(\mathbf{x},\mathbf{k})v^*(\mathbf{x},\mathbf{k})]\}. \quad (10)$$

By substituting Eq. (8) into Eq. (10) and performing proper renormalization, we can eventually reach the following analytical LHY correction [56,57,63–65]:

$$\Delta\mu(\mathbf{x}) = \int \frac{d^3\mathbf{k}}{(2\pi)^3}\tilde{V}(\mathbf{k})\left\{\frac{\varepsilon_{\mathbf{k}}}{2E(\mathbf{x},\mathbf{k})} + \frac{n_0(\mathbf{x})\tilde{V}(\mathbf{k})}{2\varepsilon_{\mathbf{k}}} - \frac{1}{2} + \frac{1}{\exp[E(\mathbf{x},\mathbf{k})/k_{\rm B}T]-1}\,\frac{\varepsilon_{\mathbf{k}}}{E(\mathbf{x},\mathbf{k})}\right\}$$
$$= \frac{32}{3}g\sqrt{\frac{a_s^3}{\pi}}[\mathcal{Q}_5(\epsilon_{\rm dd},k_c) + \mathcal{R}(\epsilon_{\rm dd},k_c)]|\Psi(\mathbf{x})|^3, \quad (11)$$

where

$$\mathcal{Q}_5(\epsilon_{\rm dd},k_c) = \frac{1}{8\sqrt{2}}\int_0^\pi d\theta\sin\theta\frac{\tilde{V}(\theta)}{g}\left[(k_c\xi_0)^3 - 3\frac{\tilde{V}(\theta)}{g}k_c\xi_0 + \left(4\frac{\tilde{V}(\theta)}{g} - (k_c\xi_0)^2\right)\sqrt{2\frac{\tilde{V}(\theta)}{g} + (k_c\xi_0)^2}\right] \quad (12)$$

and $\mathcal{R}(\epsilon_{\rm dd},k_c)$ (see the detailed expression in Appendix A) are associated with the quantum and thermal fluctuations, respectively, with $\xi_0 = 1/\sqrt{8\pi a_s n_0(\mathbf{x})}$. To get the above expression of $\mathcal{Q}_5$, we have integrated the momentum k from a cutoff k_c to infinity (again, see Appendix A). It is worth noting that the cutoff k_c is a function of θ rather than a constant due to the anisotropic property of DDI as discussed in Sec. II B. Hereafter we will focus on the case at zero temperature, where the thermal fluctuations vanish (i.e., $\mathcal{R} = 0$), and thus the LHY correction is reduced to [56,57,63–65]

$$\Delta\mu(\mathbf{x}) = \frac{32}{3}g\sqrt{\frac{a_s^3}{\pi}}\mathcal{Q}_5(\epsilon_{\rm dd},k_c)|\Psi(\mathbf{x})|^3. \quad (13)$$

We would like to point out that the cutoff k_c appearing in $\mathcal{Q}_5$ has a significant impact on the LHY correction and will be further discussed in Sec. II B. Without the cutoff (i.e., $k_c = 0$), $\mathcal{Q}_5$ can be simply approximated by a analytical function of $1 + \frac{3}{2}\epsilon_{\rm dd}^2$ by neglecting its imaginary part, which has been widely used in the research related to the effect of quantum fluctuations in quantum gases [3,6,66,80].

Here we have omitted the term related to the noncondensate density $\tilde{n}(\mathbf{x}',\mathbf{x}')$ in Eq. (4) as it is small compared to $\Delta\mu$ [64,79]. Through a similar derivation as above for $\Delta\mu$, this term can be rewritten as

$$\Delta\tilde{\mu}(\mathbf{x}) = \frac{8}{3}\sqrt{\frac{a_s^3}{\pi}}(\mathcal{Q}_3 + \mathcal{P})\int d^3\mathbf{x}'V(\mathbf{x}-\mathbf{x}')|\Psi(\mathbf{x}')|^3 \quad (14)$$

with $\mathcal{Q}_3(\epsilon_{\rm dd},k_c) = \frac{1}{2\sqrt{2}}\int_0^\pi\{\sqrt{2\frac{\tilde{V}(\theta)}{g} + (k_c\xi_0)^2}[\frac{\tilde{V}(\theta)}{g} - (k_c\xi_0)^2] + (k_c\xi_0)^3\}\sin\theta d\theta$ and $\mathcal{P}(\epsilon_{\rm dd},k_c)$ representing the quantum and thermal fluctuations, respectively. At zero

temperature ($\mathcal{P} = 0$), it reduces to

$$\Delta\tilde{\mu}(\mathbf{x}) = \frac{8}{3}\sqrt{\frac{a_s^3}{\pi}}\mathcal{Q}_3 \int \mathrm{d}^3\mathbf{x}' V(\mathbf{x}-\mathbf{x}')|\Psi(\mathbf{x}')|^3. \tag{15}$$

In Sec. III we numerically examine the effect of $\Delta\tilde{\mu}(\mathbf{x})$ and show that it merely causes a tiny shift to the critical point of a self-bound droplet in free space, which justifies the omission of this term [64,79].

B. Cutoff in momentum space

From Eq. (12) it is clear that $\mathcal{Q}_5$ inevitably has a finite imaginary part due to the anisotropic character of the DDI in the case of a vanishing cutoff $k_c = 0$. To avoid this artifact, we can choose to simply neglect the imaginary part of $\mathcal{Q}_5$ as it is small compared to the real part [80]. However, this formulation of the LHY correction leads to a deviation between the theoretical and experimental results regarding the stable regime of a single quantum droplet in free space [6].

In case of a finite-sized quantum droplet, the long-wavelength excitation is actually suppressed, and only the excitations with the momentum beyond the inverse of size of the droplet can be supported. Hence, the finite size of the droplet inherently imposes a momentum cutoff for the integration in Eq. (12). Assuming the corresponding sizes of the dipolar droplet along the polarization direction and the transverse directions are σ_z and σ_ρ, respectively, two different options of the cutoff have been suggested [4,80]:

$$k_c^{\mathrm{el,I}}(\theta) = \sqrt{k_{c,\rho}^2 \sin^2\theta + k_{c,z}^2 \cos^2\theta},$$
$$k_c^{\mathrm{el,II}}(\theta) = \left(\frac{\sin^2\theta}{k_{c,\rho}^2} + \frac{\cos^2\theta}{k_{c,z}^2}\right)^{-1/2}. \tag{16}$$

Here $k_{c,\rho} = \frac{2\pi}{\sigma_\rho}$, $k_{c,z} = \frac{2\pi}{\sigma_z}$ and θ corresponds to the angle between the momentum and the polarization directions and is spatially dependent. The superscript reflects that both parametrize an ellipse in k space. This cutoff does not depend explicitly on the spatial distribution $\boldsymbol{x}$ of the density $n_0(\boldsymbol{x})$, but rather on the predefined extent σ_ρ and σ_z. As the droplet size increases with particle number, both cutoffs vanish for $N \to \infty$. We will show later that the difference between these two cutoffs becomes indeed negligible and approaches the result without cutoff at large particle numbers. In addition to the above elliptical cutoffs, Ref. [64] empirically proposes a cutoff:

$$k_c^{\mathrm{n}}(\mathbf{x}) = \frac{\pi\sqrt{2Mgn_0(\mathbf{x})}}{2\hbar}. \tag{17}$$

Note that this cutoff includes information of the spatial distribution of the density $n_0(\mathbf{x})$, but lacks explicit information related to the interactions.

Apart from the droplet size, the healing length $\xi = \hbar/\sqrt{2Mn_0(\mathbf{x})|\tilde{V}(\mathbf{k})|}$ [13,87] also represents a natural characteristic length scale of BECs and provides an inherent limit to the excitation momentum [88–90]. It is the length scale within which the wave function can "heal" when it is pinched (or set to zero). For example, it provides a scale for the size of the vortex core. One can identify this length scale by equating the kinetic energy to the interactions. Considering Eq. (8), we see that the excitation spectrum is phononlike when $k \ll \xi^{-1}$ [i.e., $\varepsilon_{\mathbf{k}} \ll n_0(\mathbf{x})|\tilde{V}(\mathbf{k})|$] and behaves like a free particle when $k \gg \xi^{-1}$ [i.e., $\varepsilon_{\mathbf{k}} \gg n_0(\mathbf{x})|\tilde{V}(\mathbf{k})|$].

It seems that the phononlike modes shall be easier to be excited because of the low excitation energy and thus dominate the effect of fluctuations. Counterintuitively, it has been observed that the fluctuations associated with these low-momentum excitations are in fact dramatically suppressed by the correlated pair excitations carrying opposite momenta [88,89]. Therefore, we anticipate that the main contribution to the LHY correction is due to free-particle-like excitations and, for that reason, propose the following alternative cutoff using the healing length:

$$k_c^{\mathrm{h,I}}(\mathbf{x},\mathbf{k}) = \xi^{-1} = \frac{1}{\hbar}\sqrt{2Mn_0(\mathbf{x})|\tilde{V}(\mathbf{k})|}. \tag{18}$$

This implies that we neglect the contribution of the phononlike excitation modes. It is worth noting that $\tilde{V}(\mathbf{k})$ depends on only the direction of the momenta (i.e., the angle θ between $\mathbf{k}$ and the polarization direction) due to the anisotropy of the dipolar interactions. Hence, the cutoff $k_c^{\mathrm{h,I}}$ as well as the healing length is in fact independent of the modulus of $\mathbf{k}$ and varies only with the angle θ and the position in space. As $\tilde{V}(\mathbf{k})$ can be negative, we have chosen the modulus of $\tilde{V}(\mathbf{k})$ to reduce the imaginary contribution to the LHY correction. As a side note, this spatially dependent cutoff is not numerically impractical in that it is not required to evaluate it for every point in position and momentum space. As is shown in Appendix A, one merely needs to insert the specific form of the cutoff into Eq. (A7) and integrate over the momenta. Hence, as the density factors out, it is only required to calculate the coefficients $\mathcal{Q}_5$ and $\mathcal{R}$ once, without the need to recalculate them for different density profiles.

One can notice that the excitation energy $E(\mathbf{x},\mathbf{k})$ becomes imaginary if the cutoff is smaller than $\sqrt{4Mn_0(\mathbf{x})|\tilde{V}(\mathbf{k})|}/\hbar$ when $\tilde{V}(\mathbf{k}) < 0$, and thus leads to a complex LHY correction, the imaginary part of which is tiny and often neglected in previous research [1,80]. As shown in Fig. 1, we have checked that this specific choice does not lead to a significant change as compared to setting the cutoff equal to 0 (enlarging the imaginary part) or $\sqrt{4Mn_0(\mathbf{x})|\tilde{V}(\mathbf{k})|}/\hbar$ (removing the imaginary part) in domains where the interaction is negative. Namely, we introduced the piecewise functions

$$k_c^{\mathrm{h,II}}(\mathbf{x},\mathbf{k}) = \begin{cases} \frac{1}{\hbar}\sqrt{2Mn_0(\mathbf{x})\tilde{V}(\mathbf{k})} & \tilde{V}(\mathbf{k}) \geqslant 0 \\ 0 & \tilde{V}(\mathbf{k}) < 0 \end{cases} \tag{19}$$

and

$$k_c^{\mathrm{h,III}}(\mathbf{x},\mathbf{k}) = \begin{cases} \frac{1}{\hbar}\sqrt{2Mn_0(\mathbf{x})\tilde{V}(\mathbf{k})} & \tilde{V}(\mathbf{k}) \geqslant 0 \\ \frac{1}{\hbar}\sqrt{4Mn_0(\mathbf{x})|\tilde{V}(\mathbf{k})|} & \tilde{V}(\mathbf{k}) < 0 \end{cases}. \tag{20}$$

Such a cutoff associated with the healing length can also be understood from the excitation spectrum of a droplet. The above discussions are based on the LDA, which leads to an entirely continuous spectrum ranging from a low-frequency phononlike excitation domain to a high-frequency free-particle-like regime [see Eq. (8)]. However, as discussed in, e.g., Ref. [66], the excitation spectrum of a single droplet is actually composed of two distinct regimes, i.e.,

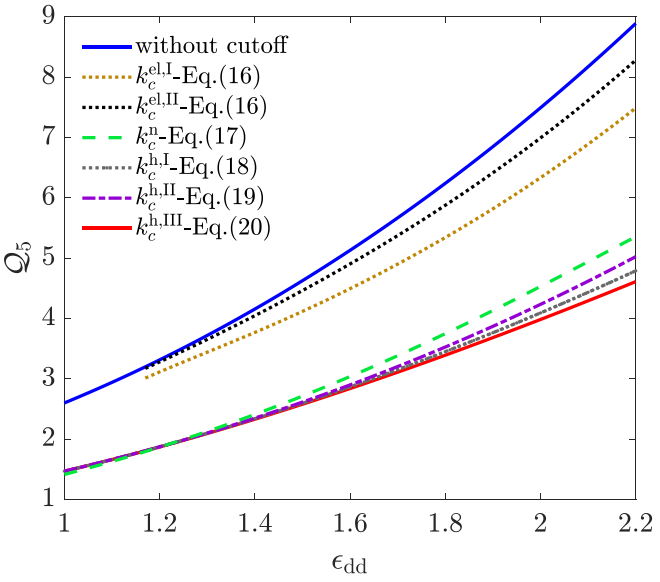

FIG. 1. The coefficient of the LHY correction $\mathcal{Q}_5$ obtained using an ellipsoidal cutoff $k_c^{\mathrm{el,I}}$ (orange) and $k_c^{\mathrm{el,II}}$ (black), a spherical cutoff k_c^{n} (green), and our proposed cutoff associated to healing length $k_c^{\mathrm{h,I}}$ (gray), $k_c^{\mathrm{h,II}}$ (purple), and $k_c^{\mathrm{h,III}}$ (red). The result without cutoff is depicted with the blue line. Only the $\mathcal{Q}_5$ obtained via $k_c^{\mathrm{h,III}}$ (red line) is purely real, while the others are complex with small imaginary parts that have been neglected in this plot.

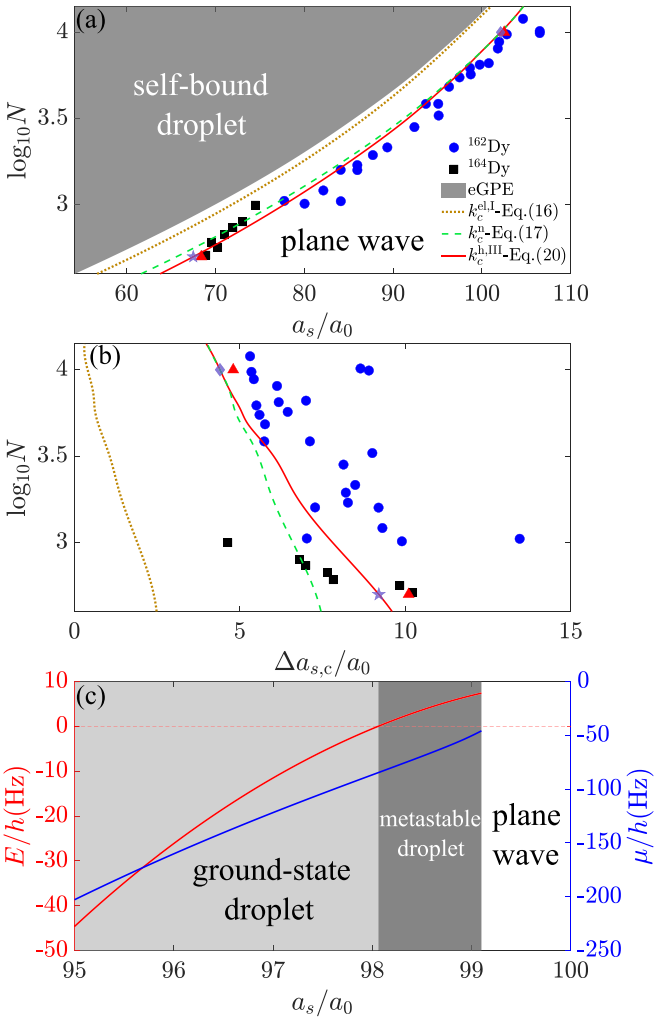

FIG. 2. (a) The phase diagram of dipolar BECs in free space. The gray region indicates the self-bound droplet phase obtained with the LHY correction without cutoff. The lines correspond to the transition points obtained using the ellipsoidal cutoff $k_c^{\mathrm{el,I}}$ (orange dashed), the spherical cutoff k_c^{n} (green dashed), and the healing length induced cutoff $k_c^{\mathrm{h,III}}$ (red), respectively. The experimental results are illustrated by the black and blue dots [6]. The red triangles depict the critical points for $N = 500$ and 10 000 obtained via $k_c^{\mathrm{h,III}}$ including $\Delta\tilde{\mu}$ [see Eq. (15)]. (b) The critical scattering length difference of each line with respect to the boundary of the gray region in (a) is plotted to represent the transition lines more clearly. (c) The energy per particle (red) and chemical potential (blue) of a droplet for $N = 7000$ is presented as function of the s-wave scattering length. The light gray zone and dark gray zone represent regimes of a stable ground-state droplet and a droplet that is metastable with respect to the plane wave, respectively.

the low-energy bound modes and the high-energy unbound modes, which approximately correspond to the aforementioned phononlike and free-particle-like modes. Additionally, it is worth noting that the cutoff beyond which the excitation spectrum is approximated employing LDA discussed here is different from the energy cutoff introduced in Ref. [86]. In Ref. [86] the energy cutoff is introduced for computational tractability for a trapped system, whereas we consider an untrapped system and discuss cutoffs that are fixed to different characteristic length scales.

To gain an intuitive understanding of the distinction between these cutoffs, we plot the coefficient of the LHY correction as a function of ϵ_{dd} (i.e., $\mathcal{Q}_5$) obtained via different options in Fig. 1. The elliptical cutoffs (16) are obtained using the size of the quantum droplet close to the phase boundary. Since this type of cutoff is size-dependent, we need to first calculate the droplet using the LHY correction without cutoff and then self-consistently iteratively update the LHY correction up to convergence. As expected, the LHY correction in this case (i.e., the orange dashed line) is gradually approaching the analytical approximation without any cutoff (i.e., the blue line) as ϵ_{dd} decreases, where the critical particle number becomes large (cf. Fig. 2) and thus leads to a nearly zero cutoff. In comparison with $k_c^{\mathrm{el,I}}$, the other elliptical cutoff $k_c^{\mathrm{el,II}}$ leads to a smaller deviation from the analytical result (not shown) [64,80]. In contrast, the spherical cutoff (17) (i.e., the green dashed line) and the cutoff induced by healing length (18)–(20) (i.e., the gray, purple, and red lines) present a noticeable difference towards lower values of the LHY correction $\mathcal{Q}_5$. Moreover, as mentioned before, the choices of the cutoff associated with the healing length in the negative $\tilde{V}(\mathbf{k})$ regime mainly lead to variation in the imaginary part of $\mathcal{Q}_5$, while the real part changes slightly.

As $\mathcal{Q}_5$ is part of the repulsive interaction, we can already foresee at this point that the droplet phase boundary will be shifted towards stronger contact interactions (i.e. larger s-wave scattering length) and lower particle number. Thus, an appropriate cutoff might lead to better agreement between theory and experiment [6]. Furthermore, the LHY correction obtained via our proposed cutoff converges to the result of

the spherical cutoff upon decreasing $\epsilon_{\rm dd}$, while it features a clear deviance to the downside upon increasing $\epsilon_{\rm dd}$. This anisotropic deviance will also manifest itself in a slightly shifted droplet phase boundary as we will discuss in the following section.

III. RESULTS AND DISCUSSIONS

To examine the reliability of our proposed cutoff, we explore the ground-state phase diagram of a dipolar condensate at zero temperature in free space using the following eGPE including the LHY correction [2–4]:

$$i\hbar\frac{\partial}{\partial t}\Psi(\mathbf{x}) = \Bigg[-\frac{\hbar^2\nabla^2}{2M} + \int V(\mathbf{x}-\mathbf{x}')|\Psi(\mathbf{x}')|^2 \mathrm{d}^3\mathbf{x}' + \frac{32}{3}g\sqrt{\frac{a_s^3}{\pi}}\mathcal{Q}_5(\epsilon_{\rm dd}, k_c)|\Psi(\mathbf{x})|^3\Bigg]\Psi(\mathbf{x}). \quad (21)$$

Here N is the total particle number of the condensate, and the wave function has been normalized to the particle number, i.e., $\int |\Psi(\mathbf{x})|^2 \mathrm{d}^3\mathbf{x} = N$. We will evaluate the LHY correction employing the different cutoffs discussed in the last section. To identify the ground state, we numerically propagate the above eGPE using imaginary time evolution (i.e., replacing t with $-it$) and renormalize the wave function after each propagation step. We use cylindrical truncation for the DDI to eliminate the influence of the periodic image caused by Fourier transformation [91,92]. Eventually the solver converges to the least damped state, unless it gets trapped at a metastable state at a local minimum of the energy. Our findings are illustrated in Fig. 2. We proceed with investigating the phase diagram in Sec. III A and subsequently discuss the error related to neglecting bound parts of the spectrum in Sec. III B.

A. Phase diagram of a single dipolar droplet

Now we would like to proceed with comparing the different approaches to the experimental data presented in Ref. [6]. We consider a dipolar BECs composed of ^{162}Dy ($a_{\rm dd} = 129a_0$ with a_0 being the Bohr radius). To scan the phase boundary of the quantum droplet, we first fix the atom number N, relax the state via imaginary time evolution, and then gradually increase the contact interaction strength by tuning the s-wave scattering length a_s up to the point where the droplet is no longer self-trapped. The results are summarized in Fig. 2(a).

As can be seen from Fig. 2(a), the stable region of the droplet (see the gray zone) predicted by the analytically approximated LHY correction without cutoff presents a deviation from the experimental observations (dots) as reported in Ref. [6]. Taking the suppression of low-momentum excitations [4,77,80] due to the finite size into account and using the elliptical cutoff to improve the LHY correction, the critical line is slightly shifted towards the experimental result as shown by the orange dashed line. This shift is more pronounced at small particle numbers, as the droplet size is smaller and thus leads to a larger finite cutoff in momentum space. However, a mismatch between theory and experiment remains.

Let us now discuss the spherical cutoff (17) and our proposed cutoff associated with the healing length Eq. (20). It appears that both of them are in good agreement with the experiment results (dots) as depicted by the green dashed line and the red line, respectively. As expected, for large particle numbers, the boundaries resulting from the cutoff associated with the healing length converges to the spherical cutoff, which is consistent with the previous analysis of the LHY coefficient in Sec. II B (cf. Fig. 1), as the anisotropy of the DDI in momentum space is reduced at small $\epsilon_{\rm dd}$. Nonetheless, the difference between them grows slightly as the atom number decreases, and we have to account for the anisotropy. Both models are in good agreement with each other and with the experimental data for relatively large particle numbers. For small particle numbers the two models diverge, and the cutoff associated with the healing length $k_c^{\rm h,III}$ appears to be closer to the experimental data. Furthermore, both results remain close to what has been found via a Monte Carlo-based simulation [93], in particular for large atom numbers. In order to highlight the difference between these boundaries, we show the critical scattering length with respect to the result obtained via the LHY correction without cutoff, i.e., $\Delta a_{s,c} = a_{s,c}^{\rm cutoff} - a_{s,c}^{\rm analytical}$, in Fig. 2(b).

A stable self-bound droplet can be either the ground state (with the lowest energy) or a metastable droplet with a higher energy than a plane wave [see the shading region in Fig. 2(c)] [79]. The boundary in Fig. 2(a) indicates the critical parameters beyond which the droplet no longer exists even as a metastable state. For illustration, the metastable region for the droplet with a particle number of $N = 7000$ is shown by the dark gray zone in Fig. 2(c). The energy per particle becomes positive in this regime. The ground state in this case corresponds to a plane wave, the energy of which is fixed at zero. In contrast, the chemical potential remains negative in the metastable region until it reaches the critical point $a_s/a_0 \approx 99.1$. Such a small absolute value of the chemical potential implies a small number of discrete excitations around the boundary of a stable self-bound droplet [66]. We will discuss bound modes in the next section.

B. Contributions of the bound modes

In the previous subsection, we have demonstrated that cutoffs have a significant impact on the phase boundary. Employing cutoffs means neglecting the contributions of all the discrete internal modes below the cutoff (i.e., the bound excitation modes of a droplet). It remains unclear whether these contributions can indeed be safely neglected. Therefore, we proceed with examining the contributions of the bound excitation modes to the LHY correction. For this purpose, we numerically calculate the Bogoliubov excitation spectrum for the self-bound droplet and then substitute it into the following equation to get the contributions of these bound modes to the LHY correction. The correction to the chemical potential can be written as

$$\Delta\mu' = -\frac{1}{|\Psi(\mathbf{x})|^2}\sum_{j\in\mathcal{B}}[E_j|v_j(\mathbf{x})|^2 + v_j^*(\mathbf{x})\mathcal{L}_0 v_j(\mathbf{x})]. \quad (22)$$

Here $\mathcal{B}$ refers to the set of all the bound modes. Equation (22) is derived without using the LDA; one can find it after some algebra via combining Eqs. (5), (6), and (9) (see Appendix B for details).

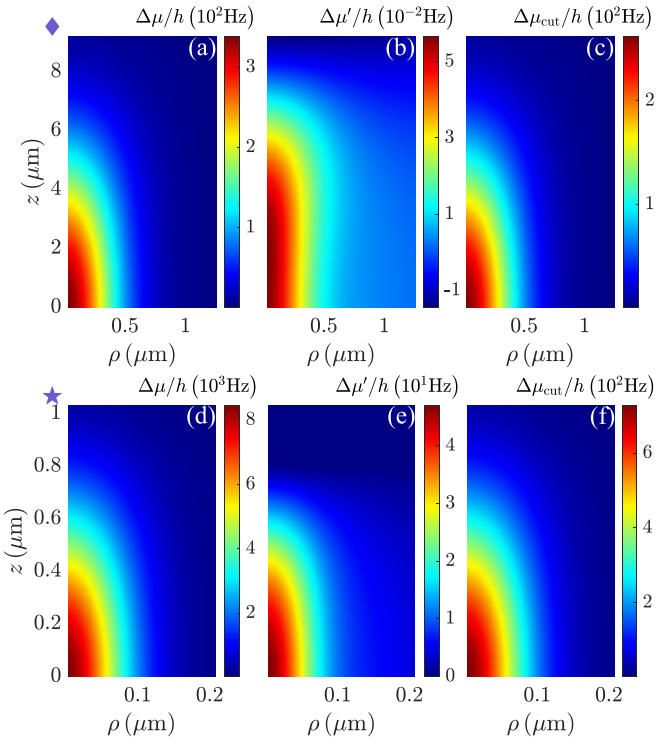

FIG. 3. The contributions of free modes and bound modes to the LHY correction near the phase transition boundary. Panels (a) and (d) show the contributions of continuous modes beyond the cutoff for $N = 10\,000$ and 500, respectively; (b) and (e) present the corresponding contributions of the discrete bound modes at $N = 10\,000$ and 500. The contributions of the momenta ranging from zero to the cutoff, $\Delta\mu_{\rm cut}$, are displayed in (c) and (f) for $N = 10\,000$ and 500, respectively. For (a, b, c) $N = 10\,000$, the s-wave scattering length is fixed at $a_s = 102.1a_0$ [marked by ♦ in Figs. 2(a) and 2(b)], while it is set to $67.5a_0$ for (d, e, f) $N = 500$ [marked by ★ in Figs. 2(a) and 2(b)].

Figure 3 shows the contributions of both free and bound excitation modes for the quantum droplets around the critical point of the phase transition. The contributions from the free modes correspond to the LHY correction obtained with the healing length-associated cutoff. Here we present the results for the droplets at a large particle number ($N = 10\,000$) and at a small particle number ($N = 500$), respectively. Since these states are close to the critical point, where the chemical potential approaches zero as shown in Fig. 2(c), there is only a small number of bound excitation modes possible, since only bound modes with a lower energy than $-\mu$ are permitted [66]. In our case, only five bound modes for $N = 10\,000$ and only two bound modes for $N = 500$ are allowed. As can be seen from Figs. 3(b) and 3(e), the contributions of these finite bound modes are several orders smaller than the contributions of the continuous free modes displayed in Figs. 3(a) and 3(d). Such a tiny contribution of the low-energy bound excitation modes justifies the cutoff for the LHY correction in the vicinity of the phase boundary. In Figs. 3(c) and 3(f) we also show the contribution of low momenta in the bound-mode regime obtained via the continuous excitation spectrum under LDA. Specifically, we integrate the momentum from 0 to q_c instead of from q_c to infinity in Eq. (A7) to obtain $\Delta\mu_{\rm cut}$. Clearly, $\Delta\mu_{\rm cut}$ is larger than $\Delta\mu'$. In other words, the LDA effectively overestimates the contribution of the low-energy discrete excitations, while the effect of the bound modes is negligible near the phase boundary. For that reason we can improve the agreement with experiment by calculating the LHY correction with an appropriately chosen cutoff.

We have also numerically checked the influence of such discrete modes on the boundary of the self-bound droplet by adding $\Delta\mu'$ to the eGPE and computing it self-consistently during the imaginary time evolution, and found that the critical line [i.e., the red line in Fig. 2(a)] barely changes. Also, we have also examined the effect of $\Delta\tilde{\mu}$ shown in Eq. (15), which is induced by the noncondensate density $\tilde{n}(\mathbf{x}', \mathbf{x}')$ and usually neglected in previous research [64,79]. By adding this term to the eGPE in Eq. (21), the critical points for the stable droplet at, e.g., $N = 500$ and 10 000 have been recalculated using our proposed cutoff [see the red triangles in Fig. 2(a)]. In comparison with the result obtained without $\Delta\tilde{\mu}$ (i.e., the red line), the shift of the critical points is negligible. A previous investigation also shows that $\Delta\tilde{\mu}$ could be actually further reduced by higher-order correlations utilizing Beliaev formalism beyond Bogoliubov approximation [94]. Hence, it is reasonable to neglect the contributions of $\Delta\tilde{\mu}$ and $\Delta\mu'$ in the eGPE, at least close to the phase boundary.

To examine the validity of our approach, we have also analyzed the bound mode contribution of a droplet state that is not so close to the transition line. Figure 4 presents an example for $N = 10\,000$ at $a_s = 50a_0$, where the critical s-wave scattering length is $\sim 102.1a_0$. In comparison with the droplet in the vicinity of the boundary [see Figs. 3(a) and 3(b)], as can be seen from the Figs. 4(a) and 4(b), the LHY correction is noticeably larger than that close to the boundary, since the peak density of the droplet as well as the quantity $a_{\rm dd}/a_s$ increases in the deep self-bound region. Furthermore, it is also worth noting that the ratio of the LHY contribution from the bound modes to that stemming from the continuous modes (i.e., $\Delta\mu'/\Delta\mu$) becomes approximately two orders of magnitude larger, but remains quite tiny $\sim 10^{-2}$ and negligible. Such an increased weight of the contribution to the LHY correction is mainly due to the large number of discrete bound excitation modes, the spectrum of which is presented in Fig. 4(e). To verify the negligibility of the bound mode effects, we first calculate the stable solution of the eGPE (21) using the LHY correction associated with the cutoff $k_c^{\rm h,III}$ [see the blue line in Figs. 4(c) and 4(d)]. Subsequently, we numerically address the discrete excitation spectrum of this stable solution. By adding the contribution of these bound modes to the LHY correction, we recalculate the stable solution of the updated eGPE via imaginary time evolution iteratively. One can see that the red dashed line (including the bound mode effect) and the blue line (without the bound mode contribution) are almost on top of each other, i.e., the density profile barely changes. That is, our proposed cutoff remains a good approximation to estimate of the effect of quantum fluctuations in a broad regime around the boundary.

However, for deeply self-bound droplets that are far from the critical point, the number of bound modes may grow quickly and result in a much larger additional contribution to the LHY correction. In this case, the effect of the bound modes might no longer be negligible and possibly needs to

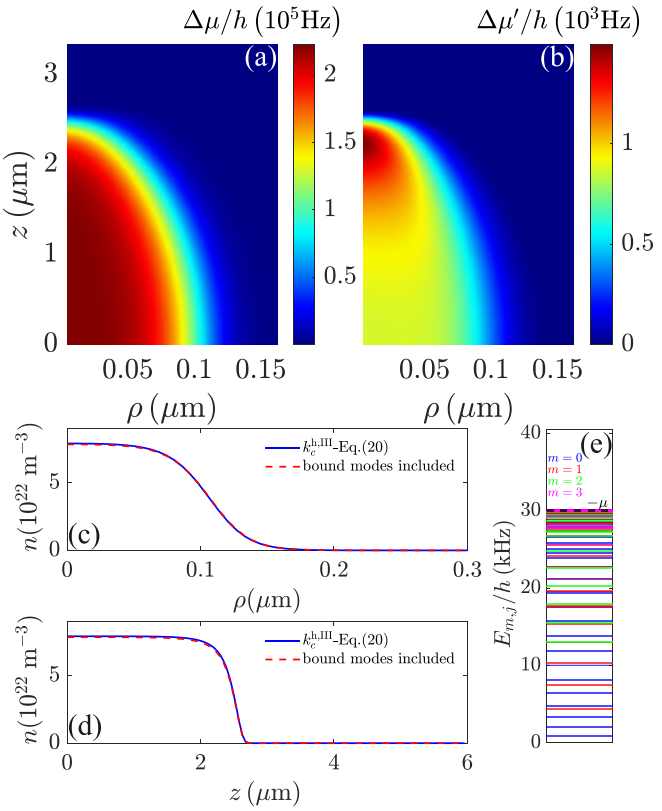

FIG. 4. The LHY correction as well as the density profile of a quantum droplet state for $N = 10\,000$ at $a_s = 50a_0$. Panels (a) and (b) present the contributions of continuous modes beyond the cutoff and that of the discrete bound modes, respectively, to the LHY correction. The density distribution of this droplet along the transverse (polarization) direction is displayed in (c) [(d)], where the blue (red) line corresponds to the ground state obtained via the LHY correction with only the continuous modes (including the discrete bound modes). The excitation spectrum of the bound modes is shown in (e).

be taken into account in Eq. (22) for an accurate description. For example, we also performed the same analysis as Fig. 4 for the unphysical situation $N = 500$ at $a_s = 15a_0$, where $\Delta\mu'/\Delta\mu \sim 0.05$ (not shown). The iterative calculation converges after two rounds. In contrast to Fig. 4, there is a discernible decrease of the droplet peak density. This is due to the fact that the discrete bound excitation modes effectively enhance the LHY correction, which behaves like a repulsive nonlinearity and thus decreases the peak density of the droplet.

IV. CONCLUSION

In this work we have discussed different possible cutoffs, including a cutoff associated with the healing length. Through numerically exploring the stability of a single self-bound droplet in free space using the different cutoffs for the LHY correction, we showed that the numerical prediction using the cutoff associated with the healing length presents a good agreement with the previous experimental observations. Moreover, we discussed the underlying physics of this cutoff. We showed that it is related to the excitation spectrum, where the inverse healing length is a natural length scale that distinguishes between the low-energy phononlike modes and the high-energy free-particle-like modes.

To further quantify the approximations, we have also investigated the effect of the bound excitation modes that are neglected by this cutoff. We showed that the contribution of those discrete modes is comparably small in the vicinity of the boundary of the droplet stable region. This appears to remain true in the deeper droplet region (small a_s) as well. We also showed that, at least in principle, in the domain of deeply self-bound droplets, the contribution of these bound modes can at some point become non-negligible.

In comparison with the numerically demanding calculation of the HFB equations, our proposed method offers an alternative simpler route that still features high accuracy. As an outlook it could also be interesting to investigate the possible cutoffs in other quantum gas systems, for example, in dipolar mixtures [5,8,9]. Furthermore, it would be interesting to include finite-temperature effects in the calculations. In addition, as the cutoff approach proposed here remains dependent on the LDA, it would be also desirable to further improve it beyond LDA in a future study.

ACKNOWLEDGMENTS

We would like to kindly thank T. Pfau for sharing the data of the work of F. Böttcher *et al.* [6] that we presented in Fig. 2(a). This work was supported by the National Key Research and Development Program of China (Grant No. 2021YFA1401700), the National Nature Science Foundation of China (Grant No. 12104359), and the Shaanxi Academy of Fundamental Sciences (Mathematics, Physics) (Grant No. 22JSY036). Y.C.Z. acknowledges the support of Xi'an Jiaotong University through the "Young Top Talents Support Plan" and Basic Research Funding as well as the High-Performance Computing Platform of Xi'an Jiaotong University for the computing facilities.

APPENDIX A: DERIVATION OF LHY CORRECTION

In this Appendix we present some details about the derivation of LHY correction that are neglected in the main text. By employing the HFB theory, we approximately expand the field operator as $\hat{\psi}(\mathbf{x}) = \Psi(\mathbf{x}) + \hat{\phi}(\mathbf{x})$ [see Eq. (4)] and substitute it into Eq. (3), and then the Hamiltonian reads

$$\begin{aligned}\hat{H} = &\int \mathrm{d}^3\mathbf{x}(\Psi^*(\mathbf{x}) + \hat{\phi}^\dagger(\mathbf{x}))h_0(\mathbf{x})(\Psi(\mathbf{x}) + \hat{\phi}(\mathbf{x})) \\ &+ \frac{1}{2}\iint \mathrm{d}^3\mathbf{x}\mathrm{d}^3\mathbf{x}'(\Psi^*(\mathbf{x}) + \hat{\phi}^\dagger(\mathbf{x}))(\Psi^*(\mathbf{x}') + \hat{\phi}^\dagger(\mathbf{x}')) \\ &\times V(\mathbf{x} - \mathbf{x}')(\Psi(\mathbf{x}') + \hat{\phi}(\mathbf{x}'))(\Psi(\mathbf{x}) + \hat{\phi}(\mathbf{x})). \qquad \text{(A1)}\end{aligned}$$

Keeping up to the third order with respect to the fluctuation operator $\hat{\phi}$ and combining the third-order terms into the first-order term via the following Hartree-Fock

factorization [64]:

$$\begin{aligned}
&\hat{\phi}^\dagger(\mathbf{x})\hat{\phi}^\dagger(\mathbf{x}')\hat{\phi}(\mathbf{x}')\\
&\quad\approx \tilde{m}^*(\mathbf{x}',\mathbf{x})\hat{\phi}(\mathbf{x}')+\tilde{n}^*(\mathbf{x}',\mathbf{x})\hat{\phi}^\dagger(\mathbf{x}')+\tilde{n}(\mathbf{x}')\hat{\phi}^\dagger(\mathbf{x}),\\
&\hat{\phi}^\dagger(\mathbf{x})\hat{\phi}(\mathbf{x}')\hat{\phi}(\mathbf{x})\\
&\quad\approx \tilde{n}^*(\mathbf{x}',\mathbf{x})\hat{\phi}(\mathbf{x})+\tilde{n}(\mathbf{x})\hat{\phi}(\mathbf{x}')+\tilde{m}(\mathbf{x}',\mathbf{x})\hat{\phi}^\dagger(\mathbf{x}),\\
&\hat{\phi}^\dagger(\mathbf{x})\hat{\phi}^\dagger(\mathbf{x}')\hat{\phi}(\mathbf{x})\\
&\quad\approx \tilde{m}^*(\mathbf{x}',\mathbf{x})\hat{\phi}(\mathbf{x})+\tilde{n}(\mathbf{x})\hat{\phi}^\dagger(\mathbf{x}')+\tilde{n}(\mathbf{x}',\mathbf{x})\hat{\phi}^\dagger(\mathbf{x}),\\
&\hat{\phi}^\dagger(\mathbf{x}')\hat{\phi}(\mathbf{x}')\hat{\phi}(\mathbf{x})\\
&\quad\approx \tilde{n}(\mathbf{x}')\hat{\phi}(\mathbf{x})+\tilde{n}(\mathbf{x}',\mathbf{x})\hat{\phi}(\mathbf{x}')+\tilde{m}(\mathbf{x}',\mathbf{x})\hat{\phi}^\dagger(\mathbf{x}'),
\end{aligned}\tag{A2}$$

Eq. (A1) is then simplified to a form that includes terms up to the second order in the fluctuation operator. For the equilibrium case, the linear term with respect to the fluctuation operator in Eq. (A1) is required to vanish, i.e., the corresponding coefficients of $\hat{\phi}$ and $\hat{\phi}^\dagger$ must be equal to zero [64,65,86]. Consequently, it leads to the following stationary eGPE:

$$\begin{aligned}
&\left[h_0(\mathbf{x})+\int \mathrm{d}^3\mathbf{x}' V(\mathbf{x}-\mathbf{x}')|\Psi(\mathbf{x}')|^2\right]\Psi(\mathbf{x})\\
&\quad+\int \mathrm{d}^3\mathbf{x}' V(\mathbf{x}-\mathbf{x}')\tilde{n}(\mathbf{x}',\mathbf{x}')\Psi(\mathbf{x})\\
&\quad+\int \mathrm{d}^3\mathbf{x}' V(\mathbf{x}-\mathbf{x}')\tilde{n}(\mathbf{x}',\mathbf{x})\Psi(\mathbf{x}')\\
&\quad+\int \mathrm{d}^3\mathbf{x}' V(\mathbf{x}-\mathbf{x}')\tilde{m}(\mathbf{x}',\mathbf{x})\Psi^*(\mathbf{x}')=0,
\end{aligned}\tag{A3}$$

i.e., Eq. (5), where we have introduced the definitions of the noncondensate density $\tilde{n}(\mathbf{x}',\mathbf{x})=\langle\hat{\phi}^\dagger(\mathbf{x}')\hat{\phi}(\mathbf{x})\rangle$ and anomalous noncondensate density $\tilde{m}(\mathbf{x}',\mathbf{x})=\langle\hat{\phi}(\mathbf{x}')\hat{\phi}(\mathbf{x})\rangle$. In order to obtain the ground-state wave function $\Psi(\mathbf{x})$, it requires us to solve these noncondensate densities. For this purpose, following the standard approach [57,86], we rewrite the fluctuation operator as a superposition of quasiparticle excitations, i.e., $\hat{\phi}(\mathbf{x})=\sum_j[u_j(\mathbf{x})\hat{\alpha}_j-v_j^*(\mathbf{x})\hat{\alpha}_j^\dagger]$, where $\hat{\alpha}_j$ ($\hat{\alpha}_j^\dagger$) is the annihilation (creation) operator of the quasiparticles satisfying Bosonic commutation relations, and the amplitudes are subject to the constraint $\int \mathrm{d}^3\mathbf{x}[u_j^*(\mathbf{x})u_k(\mathbf{x})-v_j^*(\mathbf{x})v_k(\mathbf{x})]=\delta_{jk}$. By substituting it into Eq. (A1), the second-order terms with respect to the fluctuation operator,

$$\begin{aligned}
\hat{H}_2=&\int \mathrm{d}^3\mathbf{x}\hat{\phi}^\dagger(\mathbf{x})\mathcal{L}_0\hat{\phi}(\mathbf{x})\\
&+\iint \mathrm{d}^3\mathbf{x}\mathrm{d}^3\mathbf{x}'\Psi^*(\mathbf{x})\Psi(\mathbf{x}')V(\mathbf{x}-\mathbf{x}')\hat{\phi}^\dagger(\mathbf{x}')\hat{\phi}(\mathbf{x})\\
&+\frac{1}{2}\iint \mathrm{d}^3\mathbf{x}\mathrm{d}^3\mathbf{x}'\Psi(\mathbf{x})\Psi(\mathbf{x}')V(\mathbf{x}-\mathbf{x}')\hat{\phi}^\dagger(\mathbf{x}')\hat{\phi}^\dagger(\mathbf{x})\\
&+\frac{1}{2}\iint \mathrm{d}^3\mathbf{x}\mathrm{d}^3\mathbf{x}'\Psi^*(\mathbf{x})\Psi^*(\mathbf{x}')V(\mathbf{x}-\mathbf{x}')\hat{\phi}(\mathbf{x}')\hat{\phi}(\mathbf{x}),
\end{aligned}\tag{A4}$$

with $\mathcal{L}_0=h_0(\mathbf{x})+\int \mathrm{d}^3\mathbf{x}' V(\mathbf{x}-\mathbf{x}')|\Psi(\mathbf{x}')|^2$, can be diagonalized (i.e., the terms of $\alpha_j^\dagger\alpha_k^\dagger$ and $\alpha_j\alpha_k$ vanish) when the amplitudes $u_j(\mathbf{x})$ and $v_j(\mathbf{x})$ satisfy the Bogoliubov–de Gennes (BdG) equations as shown in Eq. (5).

By solving the BdG equations, we can derive the Bogoliubov excitation spectrum. This allows us to reformulate the noncondensate densities $\tilde{n}(\mathbf{x}',\mathbf{x})$ and $\tilde{m}(\mathbf{x}',\mathbf{x})$ in terms of the excitation amplitudes $u_j(\mathbf{x})$ and $v_j(\mathbf{x})$ as demonstrated in Eq. (6).

In principle, Eqs. (4)–(6) can be solved self-consistently; however, the numerical calculations can become quite complex even for a homogeneous state [79]. Alternatively, a simpler approach involves using the local-density approximation (LDA) [56,57,64,65,82] as discussed in the main text [see the discussion about Eq. (7)]. This permits us to analytically solve the BdG equation (5) to obtain the excitation spectrum and amplitudes, as presented in Eq. (8). From the excitation amplitude solutions, we can easily derive the chemical potential shift $\Delta\mu$ [see Eqs. (9) and (10)] caused by fluctuations. By substituting Eq. (8) into Eq. (10), we can reformulate Eq. (10) as follows:

$$\begin{aligned}
\Delta\mu(\mathbf{x})=\int\frac{\mathrm{d}^3\mathbf{k}}{(2\pi)^3}\tilde{V}(\mathbf{k})\Bigg\{&\frac{\varepsilon_\mathbf{k}}{2E(\mathbf{x},\mathbf{k})}-\frac{1}{2}\\
&+\frac{1}{\exp\left[E(\mathbf{x},\mathbf{k})/k_\mathrm{B}T\right]-1}\frac{\varepsilon_\mathbf{k}}{E(\mathbf{x},\mathbf{k})}\Bigg\}.
\end{aligned}\tag{A5}$$

It is worth noting that this integral is ultraviolet divergent. Hence, to calculate the chemical shift, one needs to renormalize it by incorporating the second-order contribution of the potential $\tilde{V}(\mathbf{k})$ to the s-wave scattering length at small momenta [57,64] as follows:

$$\begin{aligned}
\Delta\mu(\mathbf{x})=\int\frac{\mathrm{d}^3\mathbf{k}}{(2\pi)^3}\tilde{V}(\mathbf{k})\Bigg\{&\frac{\varepsilon_\mathbf{k}}{2E(\mathbf{x},\mathbf{k})}+\frac{n_0(\mathbf{x})\tilde{V}(\mathbf{k})}{2\varepsilon_\mathbf{k}}-\frac{1}{2}\\
&+\frac{1}{\exp\left[E(\mathbf{x},\mathbf{k})/k_\mathrm{B}T\right]-1}\frac{\varepsilon_\mathbf{k}}{E(\mathbf{x},\mathbf{k})}\Bigg\}.
\end{aligned}\tag{A6}$$

For simplicity, we define the dimensionless momentum $q=k\xi_0$ with $\xi_0=1/\sqrt{8\pi a_s n_0(\mathbf{x})}$, and temperature $\tau=\frac{k_\mathrm{B}T}{gn_0(\mathbf{x})}$. Consequently, the integral in the equation above can be rewritten as

$$\begin{aligned}
\Delta\mu(\mathbf{x})=&4\sqrt{2}g\sqrt{\frac{a_s^3}{\pi}}|\Psi(\mathbf{x})|^3\int_0^\pi \sin\theta\,\mathrm{d}\theta\int_{k_c\xi_0}^\infty q^2\,\mathrm{d}q f(\theta)\\
&\times\Bigg\{\frac{q^2}{2\sqrt{q^2[q^2+2f(\theta)]}}+\frac{f(\theta)}{2q^2}-\frac{1}{2}\\
&+\frac{1}{\exp[\sqrt{q^2[q^2+2f(\theta)]}/\tau]-1}\\
&\times\frac{q^2}{\sqrt{q^2[q^2+2f(\theta)]}}\Bigg\}
\end{aligned}\tag{A7}$$

with $f(\theta)=\tilde{V}(\theta)/g=1+\epsilon_\mathrm{dd}(3\cos^2\theta-1)$ and k_c representing the momentum cutoff. Eventually, we obtain the following chemical potential shift led by fluctuations [56,57,63–65]:

$$\Delta\mu(\mathbf{x})=\frac{32}{3}g\sqrt{\frac{a_s^3}{\pi}}[\mathcal{Q}_5(\epsilon_\mathrm{dd},k_c)+\mathcal{R}(\epsilon_\mathrm{dd},k_c)]|\Psi(\mathbf{x})|^3,\tag{A8}$$

where

$$\mathcal{Q}_5(\epsilon_{\rm dd}, k_c) = \frac{3\sqrt{2}}{8}\int_0^\pi \sin\theta\, \mathrm{d}\theta \int_{k_c\xi_0}^\infty q^2\, \mathrm{d}q f(\theta) \times \left\{\frac{q^2}{2\sqrt{q^2[q^2+2f(\theta)]}} + \frac{f(\theta)}{2q^2} - \frac{1}{2}\right\} = \frac{1}{8\sqrt{2}}\int_0^\pi \mathrm{d}\theta \sin\theta f(\theta)[(k_c\xi_0)^3 - 3f(\theta)k_c\xi_0 + (4f(\theta) - (k_c\xi_0)^2)\sqrt{2f(\theta) + (k_c\xi_0)^2}] \quad \text{(A9)}$$

and $\mathcal{R}(\epsilon_{\rm dd}, k_c) = \frac{3}{4\sqrt{2}}\int_0^\pi \sin\theta \mathrm{d}\theta \int_{k_c\xi_0}^\infty \mathrm{d}q \frac{q^3 f(\theta)/\sqrt{q^2+2f(\theta)}}{\exp[\sqrt{q^2[q^2+2f(\theta)]}/\tau]-1}$ are associated with the quantum and thermal fluctuations, respectively. In the zero-temperature case, where $\mathcal{R} = 0$, the chemical potential shift reduces to the standard LHY correction describing the effects of quantum fluctuations, as shown in Eq. (13).

APPENDIX B: CONTRIBUTION OF THE BOUND MODES

In Appendix A we derive an analytical expression for the LHY correction using LDA. From Eq. (8) it is evident that the excitation spectrum is continuous under LDA; however, this holds true only in the high-frequency regime where excitations behave like free particles. In reality, the spectrum is discrete for the low-frequency bound modes, as demonstrated in the main text. To rigorously evaluate the contribution of the discrete bound modes, we will reanalyze starting from Eq. (9) without applying LDA.

For simplicity, let's consider the zero-temperature scenario, where Eq. (6) reduces to

$$\tilde{n}(\mathbf{x}', \mathbf{x}) = \sum_j v_j(\mathbf{x}')v_j^*(\mathbf{x}),$$
$$\tilde{m}(\mathbf{x}', \mathbf{x}) = -\sum_j u_j(\mathbf{x}')v_j^*(\mathbf{x}). \quad \text{(B1)}$$

Substituting the above expression into Eq. (9), the chemical potential shift can be rewritten as

$$\Delta\mu\Psi(\mathbf{x}) = \sum_j v_j^*(\mathbf{x})\left[\int \mathrm{d}^3\mathbf{x}' V_{\rm int}(\mathbf{x}-\mathbf{x}')v_j(\mathbf{x}')\Psi(\mathbf{x}') - \int \mathrm{d}^3\mathbf{x}' V_{\rm int}(\mathbf{x}-\mathbf{x}')u_j(\mathbf{x}')\Psi^*(\mathbf{x}')\right]. \quad \text{(B2)}$$

Meanwhile, by multiplying both sides of the second equation in Eq. (5) by $v_j^*(\mathbf{x})$ and summing over all excitations, we obtain the following relation:

$$-\sum_j E_j|v_j(\mathbf{x})|^2 = \sum_j v_j^*(\mathbf{x})\mathcal{L}_0 v_j(\mathbf{x}) + \Psi^*(\mathbf{x}) \times \sum_j v_j^*(\mathbf{x})\left[\int \mathrm{d}^3\mathbf{x}' V_{\rm int}(\mathbf{x}-\mathbf{x}')v_j(\mathbf{x}')\Psi(\mathbf{x}') - \int \mathrm{d}^3\mathbf{x}' V_{\rm int}(\mathbf{x}-\mathbf{x}')u_j(\mathbf{x}')\Psi^*(\mathbf{x}')\right]. \quad \text{(B3)}$$

Next, by combining Eqs. (B2) and (B3), we readily derive the chemical potential shift, specifically the LHY correction, without employing LDA as

$$\Delta\mu = -\frac{1}{|\Psi(\mathbf{x})|^2}\sum_j [E_j|v_j(\mathbf{x})|^2 + v_j^*(\mathbf{x})\mathcal{L}_0 v_j(\mathbf{x})]. \quad \text{(B4)}$$

Furthermore, one can easily obtain the contributions of the bound modes to the total LHY correction by simply restricting the summation only in the bound mode regime as

$$\Delta\mu' = -\frac{1}{|\Psi(\mathbf{x})|^2}\sum_{j\in\mathcal{B}} [E_j|v_j(\mathbf{x})|^2 + v_j^*(\mathbf{x})\mathcal{L}_0 v_j(\mathbf{x})], \quad \text{(B5)}$$

i.e., Eq. (22) in Sec. III B, with $\mathcal{B}$ denoting the set of all bound excitations.

[1] I. Ferrier-Barbut, H. Kadau, M. Schmitt, M. Wenzel, and T. Pfau, Phys. Rev. Lett. **116**, 215301 (2016).
[2] M. Schmitt, M. Wenzel, F. Böttcher, I. Ferrier-Barbut, and T. Pfau, Nature (London) **539**, 259 (2016).
[3] D. Baillie, R. M. Wilson, R. N. Bisset, and P. B. Blakie, Phys. Rev. A **94**, 021602(R) (2016).
[4] F. Wächtler and L. Santos, Phys. Rev. A **93**, 061603(R) (2016).
[5] A. Boudjemâa, Phys. Rev. A **98**, 033612 (2018).
[6] F. Böttcher, M. Wenzel, J.-N. Schmidt, M. Guo, T. Langen, I. Ferrier-Barbut, T. Pfau, R. Bombín, J. Sánchez-Baena, J. Boronat, and F. Mazzanti, Phys. Rev. Res. **1**, 033088 (2019).
[7] C. Mishra, L. Santos, and R. Nath, Phys. Rev. Lett. **124**, 073402 (2020).
[8] J. C. Smith, D. Baillie, and P. B. Blakie, Phys. Rev. Lett. **126**, 025302 (2021).
[9] R. N. Bisset, L. A. Peña Ardila, and L. Santos, Phys. Rev. Lett. **126**, 025301 (2021).
[10] M. Schmidt, L. Lassablière, G. Quéméner, and T. Langen, Phys. Rev. Res. **4**, 013235 (2022).
[11] F. Böttcher, J.-N. Schmidt, J. Hertkorn, K. S. H. Ng, S. D. Graham, M. Guo, T. Langen, and T. Pfau, Rep. Prog. Phys. **84**, 012403 (2021).
[12] R. Ghosh, C. Mishra, L. Santos, and R. Nath, Phys. Rev. A **106**, 063318 (2022).
[13] L. Chomaz, I. Ferrier-Barbut, F. Ferlaino, B. Laburthe-Tolra, B. L. Lev, and T. Pfau, Rep. Prog. Phys. **86**, 026401 (2023).
[14] D. Baillie and P. B. Blakie, Phys. Rev. Lett. **121**, 195301 (2018).
[15] F. Böttcher, J.-N. Schmidt, M. Wenzel, J. Hertkorn, M. Guo, T. Langen, and T. Pfau, Phys. Rev. X **9**, 011051 (2019).
[16] L. Chomaz, D. Petter, P. Ilzhöfer, G. Natale, A. Trautmann, C. Politi, G. Durastante, R. M. W. van Bijnen, A. Patscheider, M. Sohmen, M. J. Mark, and F. Ferlaino, Phys. Rev. X **9**, 021012 (2019).
[17] L. Tanzi, E. Lucioni, F. Famà, J. Catani, A. Fioretti, C. Gabbanini, R. N. Bisset, L. Santos, and G. Modugno, Phys. Rev. Lett. **122**, 130405 (2019).
[18] Y.-C. Zhang, F. Maucher, and T. Pohl, Phys. Rev. Lett. **123**, 015301 (2019).

[19] M. A. Norcia, C. Politi, L. Klaus, E. Poli, M. Sohmen, M. J. Mark, R. N. Bisset, L. Santos, and F. Ferlaino, Nature (London) **596**, 357 (2021).

[20] J. Hertkorn, J.-N. Schmidt, M. Guo, F. Böttcher, K. S. H. Ng, S. D. Graham, P. Uerlings, T. Langen, M. Zwierlein, and T. Pfau, Phys. Rev. Res. **3**, 033125 (2021).

[21] P. B. Blakie, D. Baillie, L. Chomaz, and F. Ferlaino, Phys. Rev. Res. **2**, 043318 (2020).

[22] J. Hertkorn, J.-N. Schmidt, M. Guo, F. Böttcher, K. S. H. Ng, S. D. Graham, P. Uerlings, H. P. Büchler, T. Langen, M. Zwierlein, and T. Pfau, Phys. Rev. Lett. **127**, 155301 (2021).

[23] A. Gallemí and L. Santos, Phys. Rev. A **106**, 063301 (2022).

[24] E. Poli, T. Bland, S. J. M. White, M. J. Mark, F. Ferlaino, S. Trabucco, and M. Mannarelli, Phys. Rev. Lett. **131**, 223401 (2023).

[25] T. Bland, E. Poli, L. A. Peña Ardila, L. Santos, F. Ferlaino, and R. N. Bisset, Phys. Rev. A **106**, 053322 (2022).

[26] Y.-C. Zhang, T. Pohl, and F. Maucher, Phys. Rev. A **104**, 013310 (2021).

[27] W. Kirkby, T. Bland, F. Ferlaino, and R. N. Bisset, SciPost Phys. Core **6**, 084 (2023).

[28] K. Mukherjee, M. N. Tengstrand, T. A. Cardinale, and S. M. Reimann, Phys. Rev. A **108**, 023302 (2023).

[29] M. Sohmen, C. Politi, L. Klaus, L. Chomaz, M. J. Mark, M. A. Norcia, and F. Ferlaino, Phys. Rev. Lett. **126**, 233401 (2021).

[30] T. Bland, E. Poli, C. Politi, L. Klaus, M. A. Norcia, F. Ferlaino, L. Santos, and R. N. Bisset, Phys. Rev. Lett. **128**, 195302 (2022).

[31] M. Šindik, A. Recati, S. M. Roccuzzo, L. Santos, and S. Stringari, Phys. Rev. A **106**, L061303 (2022).

[32] M. A. Norcia, E. Poli, C. Politi, L. Klaus, T. Bland, M. J. Mark, L. Santos, R. N. Bisset, and F. Ferlaino, Phys. Rev. Lett. **129**, 040403 (2022).

[33] Y.-C. Zhang and F. Maucher, Atoms **11**, 102 (2023).

[34] J. C. Smith, D. Baillie, and P. B. Blakie, Phys. Rev. A **107**, 033301 (2023).

[35] S. Halder, S. Das, and S. Majumder, Phys. Rev. A **107**, 063303 (2023).

[36] B. T. E. Ripley, D. Baillie, and P. B. Blakie, Phys. Rev. A **108**, 053321 (2023).

[37] M. Arazo, A. Gallemí, M. Guilleumas, R. Mayol, and L. Santos, Phys. Rev. Res. **5**, 043038 (2023).

[38] D. Scheiermann, L. A. Peña Ardila, T. Bland, R. N. Bisset, and L. Santos, Phys. Rev. A **107**, L021302 (2023).

[39] G. Natale, R. M. W. van Bijnen, A. Patscheider, D. Petter, M. J. Mark, L. Chomaz, and F. Ferlaino, Phys. Rev. Lett. **123**, 050402 (2019).

[40] J. Hertkorn, F. Böttcher, M. Guo, J. N. Schmidt, T. Langen, H. P. Büchler, and T. Pfau, Phys. Rev. Lett. **123**, 193002 (2019).

[41] S. Halder, K. Mukherjee, S. I. Mistakidis, S. Das, P. G. Kevrekidis, P. K. Panigrahi, S. Majumder, and H. R. Sadeghpour, Phys. Rev. Res. **4**, 043124 (2022).

[42] H. Kadau, M. Schmitt, M. Wenzel, C. Wink, T. Maier, I. Ferrier-Barbut, and T. Pfau, Nature (London) **530**, 194 (2016).

[43] D. S. Petrov, Phys. Rev. Lett. **115**, 155302 (2015).

[44] D. S. Petrov and G. E. Astrakharchik, Phys. Rev. Lett. **117**, 100401 (2016).

[45] C. R. Cabrera, L. Tanzi, J. Sanz, B. Naylor, P. Thomas, P. Cheiney, and L. Tarruell, Science **359**, 301 (2018).

[46] M. N. Tengstrand, P. Stürmer, E. O. Karabulut, and S. M. Reimann, Phys. Rev. Lett. **123**, 160405 (2019).

[47] L. Dong, D. Liu, Z. Du, K. Shi, and W. Qi, Phys. Rev. A **105**, 033321 (2022).

[48] Z. Guo, F. Jia, L. Li, Y. Ma, J. M. Hutson, X. Cui, and D. Wang, Phys. Rev. Res. **3**, 033247 (2021).

[49] V. Cikojević, L. V. Markić, G. E. Astrakharchik, and J. Boronat, Phys. Rev. A **99**, 023618 (2019).

[50] S. Gautam and S. K. Adhikari, J. Phys. B: At., Mol. Opt. Phys. **52**, 055302 (2019).

[51] H. Hu, J. Wang, and X.-J. Liu, Phys. Rev. A **102**, 043301 (2020).

[52] H. Hu and X.-J. Liu, Phys. Rev. Lett. **125**, 195302 (2020).

[53] T. D. Lee and C. N. Yang, Phys. Rev. **105**, 1119 (1957).

[54] T. D. Lee, K. Huang, and C. N. Yang, Phys. Rev. **106**, 1135 (1957).

[55] R. Schützhold, M. Uhlmann, Y. Xu, and U. R. Fischer, Int. J. Mod. Phys. B **20**, 3555 (2006).

[56] A. R. P. Lima and A. Pelster, Phys. Rev. A **84**, 041604(R) (2011).

[57] A. R. P. Lima and A. Pelster, Phys. Rev. A **86**, 063609 (2012).

[58] A. Boudjemâa, New J. Phys. **21**, 093027 (2019).

[59] X.-L. Chen, X.-J. Liu, and H. Hu, Phys. Rev. A **96**, 013625 (2017).

[60] X.-L. Chen, X.-J. Liu, and H. Hu, Phys. Rev. A **106**, 023302 (2022).

[61] X.-L. Chen, S.-G. Peng, P. Zou, X.-J. Liu, and H. Hu, Phys. Rev. Res. **2**, 033152 (2020).

[62] Q. Gu and X. Cui, Phys. Rev. A **107**, L031303 (2023).

[63] A. Boudjemâa, J. Phys. B: At., Mol. Opt. Phys. **48**, 035302 (2015).

[64] E. Aybar and M. O. Oktel, Phys. Rev. A **99**, 013620 (2019).

[65] S. F. Öztürk, E. Aybar, and M. O. Oktel, Phys. Rev. A **102**, 033329 (2020).

[66] D. Baillie, R. M. Wilson, and P. B. Blakie, Phys. Rev. Lett. **119**, 255302 (2017).

[67] A.-C. Lee, D. Baillie, R. N. Bisset, and P. B. Blakie, Phys. Rev. A **98**, 063620 (2018).

[68] I. Ferrier-Barbut, M. Wenzel, F. Böttcher, T. Langen, M. Isoard, S. Stringari, and T. Pfau, Phys. Rev. Lett. **120**, 160402 (2018).

[69] D. Petter, G. Natale, R. M. W. van Bijnen, A. Patscheider, M. J. Mark, L. Chomaz, and F. Ferlaino, Phys. Rev. Lett. **122**, 183401 (2019).

[70] S. Pal, D. Baillie, and P. B. Blakie, Phys. Rev. A **102**, 043306 (2020).

[71] T. Ilg and H. P. Büchler, Phys. Rev. A **107**, 013314 (2023).

[72] A.-C. Lee, D. Baillie, and P. B. Blakie, Phys. Rev. Res. **4**, 033153 (2022).

[73] S. Pal, D. Baillie, and P. B. Blakie, Phys. Rev. A **105**, 023308 (2022).

[74] P. B. Blakie, D. Baillie, and S. Pal, Commun. Theor. Phys. **72**, 085501 (2020).

[75] R. N. Bisset, P. B. Blakie, and S. Stringari, Phys. Rev. A **100**, 013620 (2019).

[76] M. Wenzel, F. Böttcher, T. Langen, I. Ferrier-Barbut, and T. Pfau, Phys. Rev. A **96**, 053630 (2017).

[77] J. Sánchez-Baena, C. Politi, F. Maucher, F. Ferlaino, and T. Pohl, Nat. Commun. **14**, 1868 (2023).

[78] M. Ota and G. E. Astrakharchik, SciPost Phys. **9**, 020 (2020).
[79] A. Boudjemâa and N. Guebli, Phys. Rev. A **102**, 023302 (2020).
[80] R. N. Bisset, R. M. Wilson, D. Baillie, and P. B. Blakie, Phys. Rev. A **94**, 033619 (2016).
[81] A. Griffin, Phys. Rev. B **53**, 9341 (1996).
[82] S. Giorgini, L. P. Pitaevskii, and S. Stringari, Phys. Rev. Lett. **78**, 3987 (1997).
[83] P. Courteille, R. S. Freeland, D. J. Heinzen, F. A. van Abeelen, and B. J. Verhaar, Phys. Rev. Lett. **81**, 69 (1998).
[84] S. Inouye, M. R. Andrews, J. Stenger, H.-J. Miesner, D. M. Stamper-Kurn, and W. Ketterle, Nature (London) **392**, 151 (1998).
[85] M. Theis, G. Thalhammer, K. Winkler, M. Hellwig, G. Ruff, R. Grimm, and J. H. Denschlag, Phys. Rev. Lett. **93**, 123001 (2004).
[86] S. Ronen and J. L. Bohn, Phys. Rev. A **76**, 043607 (2007).
[87] C. J. Pethick and H. Smith, *Bose–Einstein Condensation in Dilute Gases*, 2nd ed. (Cambridge University Press, Cambridge, 2008).
[88] D. M. Stamper-Kurn, A. P. Chikkatur, A. Görlitz, S. Inouye, S. Gupta, D. E. Pritchard, and W. Ketterle, Phys. Rev. Lett. **83**, 2876 (1999).
[89] J. Steinhauer, R. Ozeri, N. Katz, and N. Davidson, Phys. Rev. Lett. **88**, 120407 (2002).
[90] G. Bismut, B. Laburthe-Tolra, E. Maréchal, P. Pedri, O. Gorceix, and L. Vernac, Phys. Rev. Lett. **109**, 155302 (2012).
[91] S. Ronen, D. C. E. Bortolotti, and J. L. Bohn, Phys. Rev. A **74**, 013623 (2006).
[92] H.-Y. Lu, H. Lu, J.-N. Zhang, R.-Z. Qiu, H. Pu, and S. Yi, Phys. Rev. A **82**, 023622 (2010).
[93] R. Bombín, V. Cikojević, F. Mazzanti, and J. Boronat, Phys. Rev. A **109**, 033312 (2024).
[94] F. Zhang and L. Yin, Chin. Phys. Lett. **39**, 060301 (2022).